Material strength consideration in the design optimization of nonlinear energy harvester

Upadrashta, Deepesh; Yang, Yaowen; Tang, Lihua

2014

Upadrashta, D., Yang, Y., & Tang, L. Material strength consideration in the design optimization of nonlinear energy harvester. Journal of intelligent material systems and structures, 1-15.

https://hdl.handle.net/10356/101727

https://doi.org/10.1177/1045389X14546651

Material strength consideration in the design optimization of nonlinear energy harvester

Deepesh Upadrashta, Yaowen Yang* and Lihua Tang

School of Civil and Environmental Engineering, Nanyang Technological University, 50 Nanyang Avenue, 639798, Singapore

*Corresponding author, Email: cywyang@ntu.edu.sg

Abstract

Cantilever based piezoelectric energy harvesting from ambient vibrations is a viable solution for powering wireless sensors and low power electronic devices. For realization of such technology, it is imperative to design the energy harvester with higher power output and wider operating bandwidth. The main practical constraints on the design of harvester are system mass, volume and strength of the material. In pursuit of better performance, material strength has yet been considered in designing nonlinear energy harvesters in the literature. This paper focuses on the design optimization of nonlinear energy harvester with magnetic oscillator within the limits of allowable strain on piezoelectric material. Parametric study is carried out to find the optimal configuration of nonlinear energy harvester. Experiments show that, compared to the linear configuration, the optimized nonlinear energy harvester achieves higher power output and wider bandwidth with maximum strain on piezoelectric material below the allowable limit.

Keywords

Material strength, piezoelectric energy harvesting, optimization, nonlinear harvester, magnetic interaction

Introduction

Over the last decade, vibration energy harvesting has emerged as a potential technology for running low-powered electronic devices and wireless sensor nodes. With the increased emphasis on wireless sensor enabled monitoring applications and advancement in low-power-consuming devices, vibration energy harvesting garnered a lot of research interest. So often, energy harvesters are designed as cantilever beams with one or two piezoceramic layers covering the beam entirely or partially. Usually, a tip mass is attached to adjust the natural frequency of the harvester. Such configuration gives the maximum power only when excited at its resonant frequency. Many attempts have been made to broaden the frequency bandwidth via different approaches (Tang et al., 2010; Twiefel and Westermann, 2013). Magnetic interaction has been extensively used for broadband energy harvesting. Originally, Challa et al. (2008) used the magnetic force to alter the stiffness of the beam for tuning the natural frequency of the device. Mechanical strain induced by magnetic force was used to adjust the natural frequency of the harvester to adaptively match the excitation frequency in the literature. However, a large portion of the harvested power was utilized for the detection of frequency change and for automatic tuning (Challa et al., 2008; Zhu et al., 2008). Recently, Aboulfotoh et al. (2013) designed a self tuning resonator which autonomously adjusted the gap between the two magnets so as to match the harvester frequency to the excitation frequency. In this study, tuning of frequency from 4.7Hz to 9Hz was achieved by varying the gap between magnets from 66 to 16.7mm. However, beat phenomenon and reduction in the output were observed with slight positioning error of magnets.

Magnetic interaction is also exploited to induce nonlinear oscillations for widening the operating bandwidth. Mann and Sims (2009) designed and analyzed an electromagnetic energy harvester which uses nonlinear oscillations of magnetic levitation to obtain useful power output in the frequency range of 8-13Hz when excited at $4m/s^2$. Stanton et al. (2009) modeled and experimentally validated a nonlinear energy harvester with bi-directional tunability. Magnetic interaction around the tip mass has been tuned to obtain both hardening and softening responses and thus achieving wider bandwidth in both directions. Erturk et al. (2009) reported 200% increase in open-circuit voltage amplitude using a bistable piezomagnetoelastic structure at a rather high base acceleration of 0.5g. Very recently, Zhou et al. (2013) changed the orientation of magnets to improve the bandwidth of a nonlinear energy harvester. A frequency range of 4-22Hz with large voltage amplitude was obtained by changing the orientation of magnets from 0 to 90^0. Tang and Yang (2012) proposed a nonlinear energy harvester with magnetic oscillator to improve both power output and operational bandwidth. Under a harmonic excitation of magnitude $2m/s^2$, 100% increase in the operational bandwidth and 41% increase in the power output have been reported. Other efforts related to broadband energy harvesting can be found in the comprehensive review articles by Pellegrini et al. (2012) and Harne and Wang (2013).

Structural integrity and durability over long time are important considerations in designing energy harvester for real life applications. Inherent brittleness and fatigue due to the cyclic electromechanical loading on PZT material might cause abrupt failure of the device if material strength is not considered in the design process. In the aforementioned efforts on the design and development of nonlinear energy harvesters, material strength has not been considered in the process of achieving higher power output and wider bandwidth. Acceleration magnitudes considered in some of the works are really high which can cause premature failure of the harvester if strength constraint is not imposed in the design process (Erturk et al., 2009; Zhou et al., 2013). On the other hand, an unchecked design may result in a situation where maximum stress or strain is well below the allowable limit leading to poor utilization of the material. Wickenheiser (2011) attempted to design an energy harvester with fundamental frequency of 1.95Hz using vibrations from human walking. He arrived at a beam length of 570mm to meet the maximum strain requirements of $< 0.1\%$ and concluded that designing a compact resonant harvester from the vibrations of human walking is not possible. Shafer and Garcia (2013) derived an expression for the maximum tolerable input acceleration that a linear energy harvester can sustain based on the ultimate strength of the material and used this expression to obtain the maximum harvested power corresponding to that acceleration. Though this study provided the margin of safety of energy harvester for a given acceleration input, a more pragmatic approach would be optimizing the power output of an energy harvester for a given vibration input until the stress or strain in the material reaches its allowable limit.

Strength of some commonly used piezoelectric materials is given in Table 1. Fatigue strength values given in Table 1 are the peak values of stress allowed on the material when subjected to alternate fields or stresses. It is clearly evident from the table that the strength of piezoelectric materials rapidly decreases in case of cyclic loading and the values are much lower compared to the strength of substrate materials such as steel, aluminum, brass etc. This fact accentuates the importance of material strength of piezoelectric material in designing the energy harvester. Many researchers investigated the fatigue behavior of piezoelectric materials. Failure of piezoelectric material depends on its chemical composition, degree of brittleness (hard or soft), poling direction and also on the material used for electrodes (Schäufele and Heinz, 1996). Fett et al. (1999) investigated the behavior of soft PZT material under tensile, compression and 4-point bending tests. Narita et al. (2007) studied experimentally the influence of electric fields, poling direction and electrode material on the cyclic fatigue behavior of PZT material. Anton et al. (2010) carried out 3-point bending tests on monolithic piezoceramics PZT-5A and PZT-5H, single crystal

piezoelectric PMN-PZT and commercially packaged QuickPack devices and reported the estimates of their strengths. The results of this study can be used as the basis for the design of piezoelectric energy harvesters.

Table 1. Material strength of commonly used piezoelectric materials.

Material	Manufacturer	Product specification	Material strength	
PZT Bimorph	Morgan Advanced Materials	PZT 5A series	75.8MPa (static)	27.6MPa[1] (fatigue)
PZT patch	Channel Industries, Inc.	PZT 5804 Navy II	82.7MPa (static)	48.3MPa[2] (fatigue)
PZT wafer	MIDE Volture	V22BL	800ppm[3]	
MFC patch	Smart materials	M2807-P2	1000ppm[4]	
PMN-PT patch	TRS electrostrictors	PMN-15	85MPa[5]	

In this work, an optimal configuration of nonlinear piezoelectric energy harvester with magnetic oscillator is designed considering material strength limit. Firstly, an electromechanical model of the energy harvester is introduced with better formulation for estimating magnetic interaction in place of the commonly used dipole-dipole formulation in the literature. The maximum strain on the cantilever beam is evaluated assuming that material strains are within their linear elastic limits. Parametric study is conducted by varying the beam length and the distance between magnets to achieve higher power and bandwidth and an optimal configuration is chosen. Experiments are then carried out to validate the results from theoretical modeling.

Linear Energy Harvester

A typical piezoelectric energy harvester (PEH) is designed as a cantilever beam with a patch of piezoelectric material bonded at the fixed end and a proof mass at the free end (Figure 1). In this study, aluminum (T6) is used as substrate material and a piece of piezoelectric macro fiber composite (MFC) (Smart Materials Corp., model: M2807-P2) is bonded to the beam at its root. The portion of the aluminum beam with the patch of MFC will be referred to as composite section throughout this paper. The energy harvesting circuit with a simple resistive load R_L is considered as the main focus is on the structural aspects of the energy harvester. The governing electromechanical equations for the PEH subjected to base motion $u_0(t)$ are derived considering single-mode approximation and using the Hamiltonian principle following similar procedure described by Hagwood et al. (1990), Sodano et al. (2004) and Elvin and Elvin (2009).

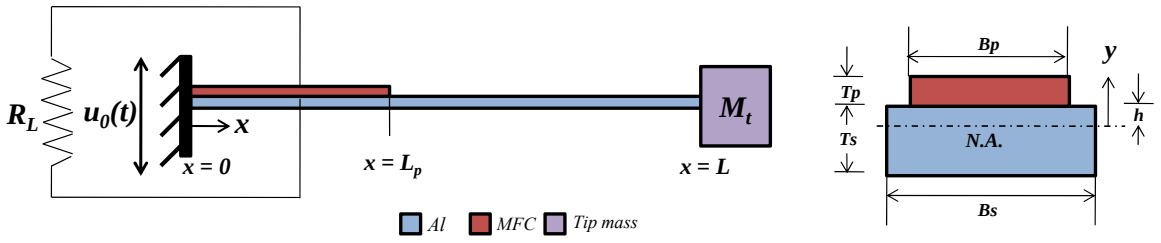

Figure 1. Schematic representation of a cantilever linear PEH.

$$M\,\ddot{u}(t) + C\,\dot{u}(t) + K\,u(t) + \Theta\,V(t) = F(t) \tag{1}$$

$$\frac{V(t)}{R_L} + C^s\,\dot{V}(t) - \Theta\,\dot{u}(t) = 0 \tag{2}$$

In equations (1) and (2), $V(t)$ is the voltage across the resistor R_L; $u(t)$ is the modal displacement in single mode approximation, where displacement $w(x,t)=u(t)\emptyset(x)$; M, K, C and Θ are the modal mass, stiffness, damping and electromechanical coupling terms, respectively; C^S is the clamped capacitance of the piezoelectric patch; and $F(t)$ is the mechanical forcing due to the base acceleration. The damping coefficient C is usually measured experimentally. The definitions of other terms are given below. Throughout this paper subscripts *s*, *p* and *c* corresponds to substrate, piezoelectric material and composite sections, respectively.

$$M = \int_0^L m_*(x)\,\emptyset(x)^2 dx + M_t\emptyset(L)^2 \tag{3}$$

$$K = \int_0^L EI_*(x)\,\emptyset''(x)^2 dx \tag{4}$$

$$\Theta = -\int_{v_p} y\emptyset''(x)\,e_{31}\psi(y)dv_p \tag{5}$$

$$F(t) = -\left(M_t\emptyset(L) + \int_0^L m_*(x)\,\emptyset(x)dx\right)\ddot{u}_0(t) \tag{6}$$

Here, m and EI are mass per unit length and flexural rigidity of the beam. The '*' corresponds to the specific portion of the beam, either composite section or substrate. M_t is the tip mass. e_{31} is piezoelectric stress constant. The spatial variable x is measured from the root and y is measured from the neutral axis of the beam, as shown in Figure 1. L is the length of the beam. The function $\psi(y)$ defines the electric field over the piezoelectric element which is assumed to be constant (Sodano et al., 2004). The integral in the equation (5) is evaluated over the volume of the piezoelectric material (v_p) in the composite section. $\emptyset(x)$ is the mode shape normalized to unity corresponding to the first natural frequency of the beam and expressed in two parts as the cantilever beam is covered partially by the piezoelectric material.

$$\emptyset(x) = \begin{cases} \emptyset_c(x) & for\ 0 \le x \le L_p \\ \emptyset_s(x) & for\ L_p \le x \le L \end{cases} \tag{7}$$

Differential eigenvalue problem for this configuration is

$$\begin{cases} (EI)_c\emptyset_c^{iv} - m_c\omega^2\emptyset_c = 0 \\ (EI)_s\emptyset_s^{iv} - m_s\omega^2\emptyset_s = 0 \end{cases} \tag{8}$$

The solution form for the mode shape is

$$\begin{cases} \emptyset_c(x) = A_1 cos(\beta_1 x) + B_1 sin(\beta_1 x) + C_1 cosh(\beta_1 x) + D_1 sinh(\beta_1 x) \\ \emptyset_s(x) = A_2 cos(\beta_2 x) + B_2 sin(\beta_2 x) + C_2 cosh(\beta_2 x) + D_2 sinh(\beta_2 x) \end{cases} \tag{9}$$

with the following geometric and natural boundary conditions to determine the values of β_1 and β_2 which give non- trivial $\emptyset(x)$:

$$\begin{cases} \emptyset_c(0) = 0,\ \emptyset_c'(0) = 0,\ \emptyset_c(L_p) = \emptyset_s(L_p),\ \emptyset_c'(L_p) = \emptyset_s'(L_p) \\ (EI)_c\emptyset_c''(L_p) = (EI)_s\emptyset_s''(L_p),\ (EI)_c\emptyset_c'''(L_p) = (EI)_s\emptyset_s'''(L_p) \\ (EI)_s\emptyset_s''(L) = I_t\,\omega^2\,\emptyset_s'(L),\ (EI)_s\emptyset_s'''(L) + \omega^2 M_t\emptyset_s(L) = 0 \end{cases} \tag{10}$$

where I_t is the rotational inertia of tip mass M_t.

Nonlinear Energy Harvester

Tang and Yang (2012) proposed a nonlinear energy harvester in which the conventional PEH was aided by magnetic oscillator to achieve both wider bandwidth and higher power output. As shown in Figure 2, a subsystem of magnetic mass-spring-damper was introduced in the enclosure carrying a PEH with a magnet at its tip. The dynamics of PEH is altered by the presence of the magnetic oscillator, resulting in improvement of bandwidth and power. For theoretical study, the magnetic oscillator is assumed as an additional cantilever with a tip mass carrying a magnet. The distance d between the two embedded magnets strongly influences the nonlinear characteristics of PEH. The electromechanical equations of this nonlinear harvester are given below:

$$M_1\,\ddot{u}_1(t) + C_1\,\dot{u}_1(t) + K_1\,u_1(t) + \Theta\,V(t) - F_{mag} = F_1(t) \quad (11)$$

$$M_2\,\ddot{u}_2(t) + C_2\,\dot{u}_2(t) + K_2\,u_2(t) + F_{mag} = F_2(t) \quad (12)$$

$$\frac{V(t)}{R_L} + C^s\,\dot{V}(t) - \Theta\,\dot{u}_1(t) = 0 \quad (13)$$

where subscripts 1 and 2 refer to the parameters of PEH and magnetic oscillator, respectively. The effective modal terms for each beam are determined as explained in the previous section. F_{mag} is the magnetic force which varies with the relative displacement between the PEH and the oscillator. In their study, Tang and Yang (2012) approximated the magnetic force as interaction between dipoles. In this article, a better formulation is used to account for the magnetic force which predicts the response of PEH more accurately.

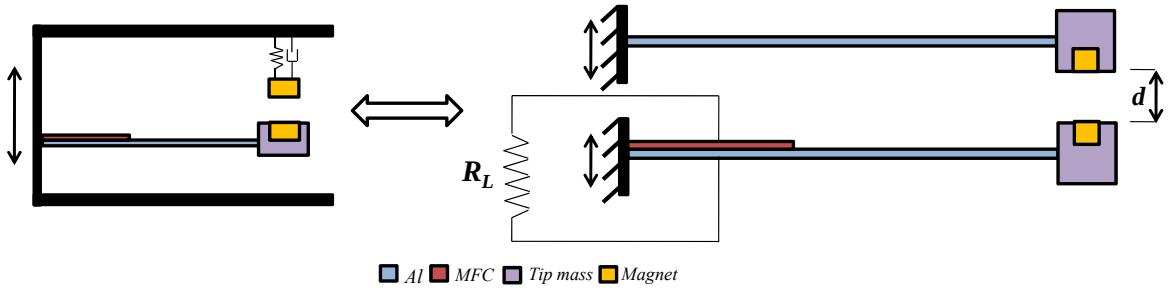

Figure 2. Schematic representation of nonlinear piezoelectric energy harvester with magnetic oscillator.

Magnetic Force

For analyzing nonlinear energy harvesters with magnetic interaction, the dipole-dipole approximation has been used extensively in the literature (Challa et al., 2008; Stanton et al., 2009; Tang et al., 2012; Stanton et al., 2010). The force between the magnetic dipoles is given by:

$$F_{dipole} = \frac{3\,\mu_0 m_1 m_2}{2\pi\,d^4} \quad (14)$$

where m_1 and m_2 are the moments of magnetic dipoles; μ_0 is the vacuum permeability. The dipole model is accurate only when the distance between magnets is sufficiently large. As shown in the later part of this section, the dipole model gives quite erroneous results within the distances normally used in energy harvester designs. Experiments have been carried out and results have

been curve fitted to establish accurate relation between the magnetic force and the separation distance (Mann and Sims, 2009; Alphenaar et al., 2010; Aboulfotoh et al., 2013; Zhou et al., 2013). The curve fitted expressions were used in governing equations to study the behavior of the harvester. Though this method evaluates the magnetic interaction accurately, conducting experiments is time consuming. Experiments have to be repeated if magnets of different dimensions and strength are used. Thus, it is highly desired to have a good formulation to evaluate the magnetic force. In this section, a closed-form expression for computing the force between cylindrical magnets available in the literature is presented and compared with the extensively used dipole model. Additionally, other available solutions for evaluating the interaction between permanent magnets are discussed in the view of growing interest in the usage of magnetic interaction for broadband energy harvesting.

The closed-form expression of the interaction force between two identical and axially aligned magnetic disks was developed to calculate levitation force for radial and axial bearing configurations (Furlani, 2001). There are various techniques to analyze permanent magnets such as representing magnets by equivalent magnetic charges or currents, application of the Maxwell's stress tensors, the principle of virtual work and the use of Kelvin's formula (Agashe and Arnold, 2008). In his study, Furlani (2001) modeled the magnets as volumes of distributed magnetic charges and the force between the two charge distributions was computed. In this model, the magnets are assumed to be of fixed and uniform polarization. Integral expressions in the model to solve for the magnetic field and force are evaluated by discretizing the magnets into mesh of elements and contribution from each element is summed up. Due to the geometric symmetry of the magnets, equations are derived in cylindrical coordinates. The force between two identical and axially aligned magnetic disks is given as:

$$F_{mag} = \frac{\mu_0}{4\pi} J^2 \left\{\frac{\pi\left(R_2^2 - R_1^2\right)}{N_r N_\theta}\right\}^2 N_\theta \sum_{q=0}^{2} \sum_{i=1}^{N_r} \sum_{i'=1}^{N_r} \sum_{j'=1}^{N_\theta} \frac{(-1)^q \alpha_q d_q}{\left[r_i^2 + r_{i'}^2 - 2 r_i r_{i'} Cos\left(\theta_{j'}\right) + h_q^2\right]^{3/2}} \quad (15)$$

where J is the saturation magnetization; R_1 and R_2 are the inner and outer radius of magnet, respectively; N_r and N_θ are the number of elements in the radial and circumferential directions, respectively. Other parameters are defined as follows:

$$\theta_{j'} = (j' - 1)\Delta\theta + \frac{\Delta\theta}{2} \qquad \left(j' = 1,2, \dots, N_\theta\right),$$

$$\Delta\theta = \frac{2\pi}{N_\theta},$$

$$r_i = \frac{R(i+1) + R(i)}{2} \qquad (i = 1,2, \dots, N_r),$$

$$r_{i'} = \frac{R(i'+1) + R(i')}{2} \qquad \left(i' = 1,2, \dots, N_r\right),$$

$$R(i+1) = \sqrt{R(i)^2 + \frac{R_2^2 - R_1^2}{N_r}} \quad (i = 1,2, \dots, N_r),$$

$$R(i'+1) = \sqrt{R(i')^2 + \frac{R_2^2 - R_1^2}{N_r}} \quad (i' = 1,2, \dots, N_r),$$

$$d_q = d + q\, t_q \quad (q=0,1,2),$$

$$\alpha_q = \begin{cases} 1 & q = 0, \\ 2 & q = 1, \\ 1 & q = 2. \end{cases}$$

where, t_q is the thickness of magnet. Since the above solution is obtained through discretization, its accuracy depends on the number of elements used. It is found out that with mesh resolution of N_r=25 and N_θ=25, the discretization error in the evaluation of magnetic force is of the order 0.001N. Higher mesh resolution unnecessarily increases the computational time as the magnetic force is repeatedly calculated in solving the governing equations numerically.

To evaluate the accuracy of different models, the magnetic forces calculated using the above closed-form solution and the dipole model are compared with the results from finite element analysis (FEA), which is carried out with magnetostatic module in Comsol Multiphysics using 3D models of magnets. Cylindrical Neodymium (NdFeB) magnets of radius 2mm, thickness 3mm and magnetization 828KA/m are used for simulation. The effective magnetic moment computed assuming magnets as dipoles is 0.0192Am^2. Force values computed using equations (14), (15) and FEA for a series of separation distances are compared in Figure 3.

From Figure 3, it is very clear that the closed-form solution given by the charge model matches well with the FEA results whereas the dipole model predicts much higher values when the separation distance becomes smaller. Force predicted by dipole model starts deviating from results of FEA and closed-form solution considerably when the spacing between magnets is 7mm. At 5mm of separation distance between magnets, error from the dipole model is almost 200%. Note that, the separation distance d shown in Figure 2 is the distance between magnets at rest. During the motion of beams under base acceleration, tip masses along with embedded magnets oscillate and interact at even closer distances. Higher base acceleration results in closer spacing of magnets around 5mm or less and the dipole model in such case would result in erroneous results. Hence it is recommended that the dipole model should not be used when the distance between magnets is close during the motion (less than 7mm) so as to avoid inaccurate prediction of response of the energy harvester. Moreover, the force expression (15) derived in terms of magnet material properties, dimensions and spacing of magnets is convenient to use, which facilitates rapid parametric studies.

Cylindrical and cuboidal magnets in various configurations have been used for broadband energy harvesting. There are other analytical solutions in the literature for computing the force between permanent magnets. Agashe and Arnold (2008) derived analytical expressions for axial and lateral forces between cylindrical and cuboidal magnets as functions of separation distance and dimensions of magnets. The closed form expressions were derived using the Kelvin's formula and the equivalent currents approach. The analytical expressions involving hypergeometric expansion used for evaluating the elliptic integrals are complex and computationally more expensive than the closed form expression given by Furlani (2001). Ravaud et al. (2010) has given analytical expressions for magnetic parameters such as field, force, torque and stiffness in cylindrical magnets and coil. The expressions are based on the elliptic integrals without any simplification and the integrals need to be solved in Matlab or Mathematica. These expressions are more accurate than the other closed form expressions discussed above as there is no simplifications used for evaluating the elliptical integrals. However, the repeated evaluation of elliptical integrals while solving the dynamic equations (11) to (13) is highly computationally expensive. Furthermore, the closed form expression given by Furlani (2001) gives very good accuracy for the separation distances considered in this work. Robertson et al. (2011) presented the original equation proposed by Ravaud et al. (2010) in a more compact form using fewer

parameters but it still requires the evaluation of elliptical integrals. Therefore, the closed form expression given by Furlani (2001) is used in this work as it is computationally less expensive and easy to implement.

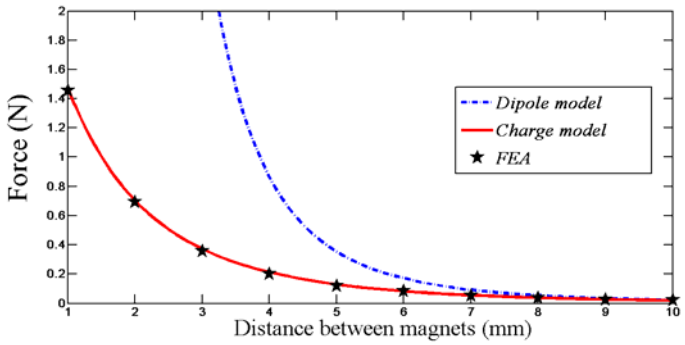

Figure 3. Force between cylindrical magnets versus separation distance.

Power Output of Linear and Nonlinear PEH

Using the closed-form expression for magnetic force presented in the last section and equations (11) to (13), dynamics of nonlinear energy harvester is studied in this section. The governing differential equations are written in the state space form and solved by numerical integration in MATLAB. The state space form of the governing equations is given in Appendix.. Attractive configuration of magnets is considered for studying the behavior of the harvester. Natural frequencies of 27.8 Hz and 24.4 Hz are considered for PEH and magnetic oscillator, respectively, similar to the original design proposed by Tang and Yang (2012). Harmonic base acceleration a_{rms} of magnitude 2m/s^2 is used in this work. In fact, other frequency range and different base acceleration can be considered depending upon the input vibration characteristics for which the harvester has to be designed. The geometric parameters of the beams considered for simulation are also of the original design and are given in Table 2. The performance of harvester is evaluated for two different separation distances between magnets i.e. d=10 mm and 8 mm. Additionally, the maximum strain on the piezoelectric material will be evaluated for the considered configurations in the subsequent section. The results will prompt for a parametric study to find the nonlinear harvester configuration that meets the material strength criteria and also has better performance.

The tip masses weighing 4.6g and 6g are used to achieve natural frequencies of 27.8Hz and 24.4Hz for the PEH and magnetic oscillator, respectively. While deriving the modal terms, the tip mass is assumed as point mass with I_t=0. It is assumed that rotations of tip masses are small enough such that the magnets are axially aligned. A load resistance of 400kΩ is considered in the simulation. Nonlinear behavior of the harvester is studied when magnets are separated by 8mm and 10mm. The separation distance (8mm or 10mm) refers to the distance between magnets when the beams are stationary. Smaller distances are not considered because of snapping action of magnets. Usually, magnets snap each other (sudden movement) at a certain critical distance. In this design, the attraction force between magnets is resisted by the beams (K*δ). Here, K is the stiffness of the beam and δ is the tip deflection. When the two tips are close enough (during motion) so that magnetic force is more than the resistance from beams, the two magnets snap each other. This makes the energy harvester useless and large force is required to separate magnets. Therefore, it is very crucial to design harvesters such that the relative spacing during motion is sufficiently large enough to avoid snapping action of magnets.

Table 2. Parameters of nonlinear energy harvester with magnetic oscillator.

Parameter	Piezoceramic	Substrate
Material	MFC 2807-P2	Aluminum
Length (L_p, L) (mm)	28	70
Width (B_p, B_s) (mm)	7	10
Thickness (T_p, T_s) (mm)	0.2	0.6
Elastic modulus (E_p, E_s) (GPa)	30.336	68.9
Mass density (ρ_p, ρ_s) (kg/m^3)	5440	2700
Piezoelectric constant (e_{31}) (C/m^2)	-5.16	---
Capacitance (C^S) (nF)	12.4	---

Figure 4 shows the power output from the linear and the nonlinear PEH. Power delivered to the electrical load is given by V^2_{rms}/R_L, where V_{rms} is the RMS voltage output obtained from solving the governing equations (11) to (13). It is conspicuous that PEH with magnetic oscillator provides both wider bandwidth and higher output power when compared to linear PEH. The main features of nonlinear harvester are reflected in the increased power output at the resonant frequency and the wider bandwidth because of the presence of another peak near the resonance frequency of magnetic oscillator. The maximum power output from the nonlinear PEH is 1579μW, showing 46% increase when compared to the maximum power output from the linear PEH (1080μW). The bandwidth corresponding to 100μW power output has also shown 30% increase from the linear PEH (3Hz) to the nonlinear PEH (3.9Hz). The reason for enhancement in performance is due to the dynamics of added magnetic oscillator to the system. When the frequency is swept near resonant frequencies of beams (27.8Hz and 24.4Hz), energy from one beam (oscillator) is transferred to the other (harvester) through magnetic interaction, resulting in better performance. Power and bandwidth are further increased through intensification of magnetic nonlinearity by reducing the spacing between magnets from 10 to 8mm. For d=8mm nonlinear configuration, the maximum power output of 2137μW and the bandwidth of 4.3Hz have been achieved, showing 98% and 43% increase, respectively, as compared to the linear configuration.

The presence of nonlinear magnetic force makes harvester a duffing model. But, the nonlinear behavior of a duffing model becomes apparent only when the harvester experiences significant amplitude. The base acceleration considered in this work is 2 m/s^2 (RMS) which is not sufficient to induce higher amplitudes. From Figure 4, it is evident that the bending of response curves of the harvester which is hall mark feature of the duffing oscillator is not observed. However, the magnetic force influences linear stiffness and results in shift of the resonant frequency. The attractive magnetic force has a softening effect on the resonant frequency of the harvester. The peak of power output slightly moves towards the left of the resonant frequency of linear PEH as the attraction force between magnets reduces the stiffness of the beam. The shift in the resonant frequency increases with closer spacing of the magnets as expected. The resonant frequencies of nonlinear harvester shift by 0.6 Hz and 1.2 Hz to the left of linear harvester for d=10 and d= 8 mm, respectively. The second peak of power output corresponding to the resonant frequency of the oscillator also shifts to the left. It should be mentioned that the higher power output and wider bandwidth are achieved not because of the nonlinear stiffness induced by the magnetic force, but the transfer of energy from the oscillator to the harvester near resonant frequencies.

The power output using the dipole formulation is also plotted for the purpose of comparison. For the case of d=10 mm, power output value computed using dipole model (1879μW) is much higher compared to the value computed using charge model (1579μW). Power output of the case

d=8mm using dipole model is not plotted as the model predicts higher magnetic force, resulting in higher tip deflections. Near the resonant frequency of PEH or oscillator, the initial spacing of magnets (8mm) is closed by relative displacement of magnets (u_1-u_2) and resulted in sticking of the magnets. For the same configuration, charge model predicts maximum relative displacement as 3.36mm and maximum power output of 2137μW. The large error in prediction of the power and displacement concludes that the dipole model cannot be used when magnets are interacting at closer distances.

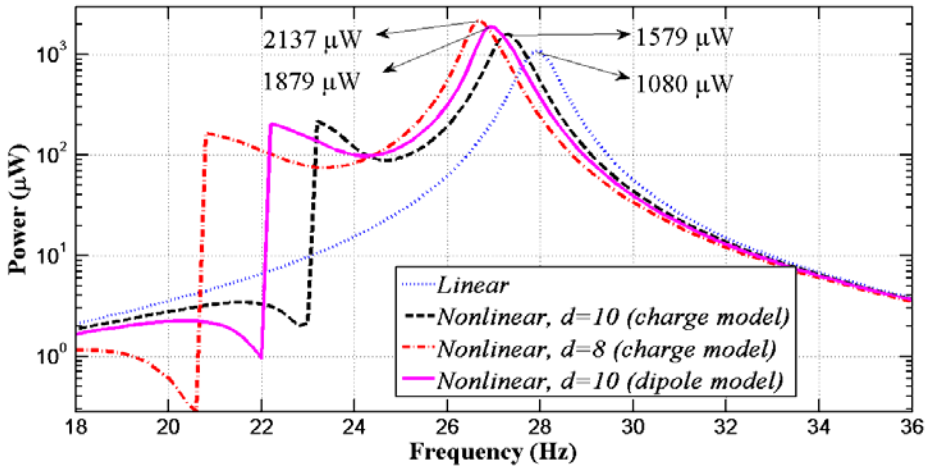

Figure 4. Power output from the linear and the nonlinear energy harvesters at a_{rms}=2m/s^2 from simulation.

Maximum strain in PEH

In this section, we derive the maximum strain on the cantilevered PEH for material strength consideration in design. The prediction of power output would be meaningless if the maximum strain in the PEH exceeds the allowable limit. Generally piezoceramics have lower strength than the substrate materials and are more susceptible to failure due to their brittleness. Hence we analyze the maximum strain in the piezoelectric material. Assuming that the mechanical perturbations are small and the material is under small electric field conditions, the constitutive relations for the piezoelectric material are (IEEE Standard, 1987):

$$\begin{bmatrix} \epsilon \\ D \end{bmatrix} = \begin{bmatrix} s^E & d^c \\ d^d & \varepsilon^\sigma \end{bmatrix} \begin{bmatrix} \sigma \\ E^f \end{bmatrix} \tag{16}$$

In the above equation, ϵ is the strain which depends on both stress (σ) and electric field (E^f). Strain and electric displacement (D) are related to stress and electric field through elastic compliance (s^E), dielectric permittivity (ε^σ) and piezoelectric constants(d^c, d^d). The superscripts on elastic compliance and dielectric permittivity denote that these constant are evaluated at constant electric field and constant stress respectively. The superscripts on piezoelectric constants refer to direct and converse effect of piezoelectric materials but the constants are numerically the same.

In deriving the maximum strain on the cantilever beam, we assume that the aluminum substrate and MFC patch are perfectly bonded together and the effect of epoxy layer between them is neglected. The axial strain in the cantilever beam can be written from the constitutive equations (16) as

$$\epsilon_x = s^E \sigma_x + d_{31} E^f \tag{17}$$

The first term on the right-hand side in the above equation refers to the strain contribution from the deflection of the beam. The compliance is equal to the inverse of elastic modulus ($s^E=1/E_x$) and the bending stress is given by the flexure formula ($\sigma_x=-M_z y/I$). Sign convention of bending moment (M_z) is that the positive moment produces positive curvature. The bending moment can be approximated as $K\delta(L-x)$. The tip deflection of the beam can be obtained as $u(t)\emptyset(L)$. With the above relations, the first term in equation (17) can be written as

$$s^E \sigma_x = \frac{-Ku(t)\emptyset(L)y(L-x)}{(EI)_x} \tag{18}$$

The second term in equation (17) is the strain caused by the electric field across the piezoelectric element. d_{31} is the piezoelectric constant for 31 mode, given as $d_{31}=e_{31}/E_p$, where E_p is the elastic modulus of piezoelectric material in the axial direction. The electric field across the piezoelectric element is assumed to be uniform, given as $E^f=-V(t)/T_p$ (Sodano et al., 2004). The maximum strain occurs on the farthest layer from neutral axis at the root of beam, given by:

$$\epsilon_{max} = \frac{-Ku_{max}\emptyset(L)(h+T_p)L}{(EI)_c} - \frac{e_{31}V}{E_p T_p} \tag{19}$$

where

$$h = \frac{T_s}{2}\left[\frac{1-\frac{E_p}{E_s}\frac{B_p}{B_s}\left(\frac{T_p}{T_s}\right)^2}{1+\frac{E_p}{E_s}\frac{B_p}{B_s}\frac{T_p}{T_s}}\right]$$

$$(EI)_c = \frac{1}{3}E_s B_s(T_s-h)^3 + \frac{1}{3}E_s B_s h^3 + \frac{1}{3}E_p B_p(T_p+h)^3 - \frac{1}{3}E_p B_p h^3$$

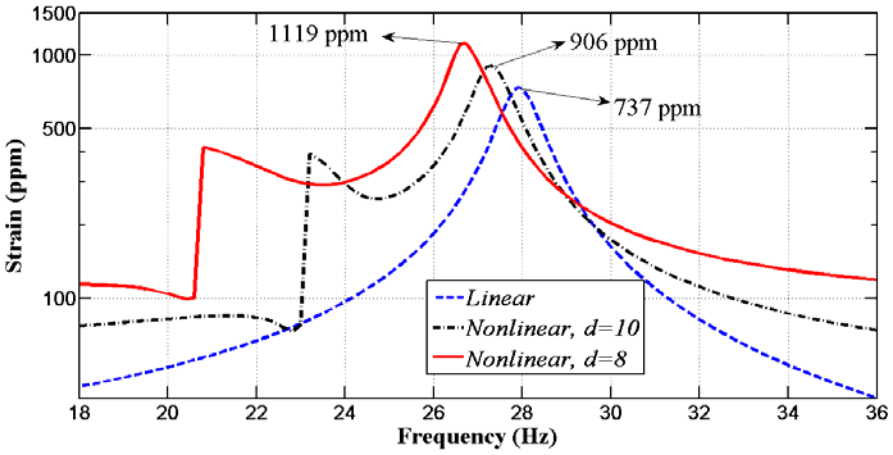

Figure 5. Maximum strain in piezoelectric material of linear and nonlinear harvesters excited at a_{rms}=2m/s^2 from simulation.

The experiments performed at NASA Langley Research Center has shown no reduction in the performance of MFC actuator up to 100 million cycles under in-plane strains of -500 to 1500ppm (Wilkie et al., 2002). Though MFC can sustain up to tensile strain of 4500ppm[4], the durability of the material under cycling loading decreases rapidly with higher amplitudes of strain. The

operating life time of MFC actuator reduces from 10^9 cycles to 10^7 cycles when applied voltage increases from 1kV to 2kV (peak-to-peak)[4]. Furthermore, the assumptions in using the piezoelectric constitutive equations and in deriving the maximum strain on the beam require the material to be straining under the elastic limit. Taking into account above all the considerations, 1000ppm[4] (both in tension and compression) is considered as the upper limit of the allowable strain in this work. The fatigue strength of the aluminum (T6) substrate used in this study is 1400ppm[6] which is higher than the strength of MFC. Moreover, the distance of the extreme aluminum layer from the neutral axis (0.337mm) is less than the distance of the extreme piezoceramic layer (0.463mm) from the neutral axis in the composite section of the beam. Hence aluminum undergoes less strain than the piezoceramic material and operates within the allowable limit. It is advisable to use specially treated metal sheets for substrates which have higher fatigue strength.

The maximum strain in piezoelectric material on cantilever beams of the linear and nonlinear PEH is shown in Figure 5. It is clear from figure that the linear PEH and the nonlinear PEH with 10mm magnetic spacing are operating within the allowable limit of strain. But, the maximum strain of the nonlinear PEH with 8mm magnet spacing exceeds the upper limit. Closer spacing of magnets (8mm) provides better performance in terms of power and bandwidth (Figure 4), but it increases the strain in the piezoelectric material to an unacceptable value. On the other hand, the nonlinear PEH with 10mm magnet spacing is safe but inferior in performance. Therefore, parametric study is desired to seek an optimal configuration of nonlinear PEH that gives better performance and at the same time operates within the allowable strain limit.

Parametric study

In this parametric study, performance characteristics of nonlinear PEH for various beam lengths are evaluated. For each length of the beam, the tip masses are adjusted such that the natural frequencies of PEH (27.8Hz) and magnetic oscillator (24.4Hz) are kept unchanged. Again, two cases of separation distance between magnets i.e. 8mm and 10mm are considered and the base acceleration is $2m/s^2$, same as the previous sections. The values of damping ratio, required to investigate the behavior of PEH, are experimentally measured for different beam lengths using the logarithmic decrement method (Leonard, 2001). The experimentally measured damping values are shown in Figure 6.

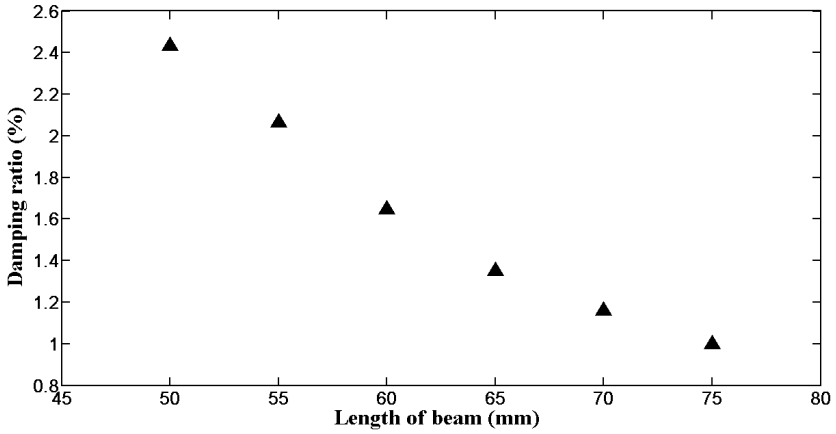

Figure 6. Damping ratio for different beam lengths.

Figure 7 illustrates the power output and the maximum strain for various beam lengths. For the sake of legibility, the results for nonlinear PEH with d=8mm and d=10mm are only plotted. For better comparison, the results of linear PEH and two cases of nonlinear PEH with different beam lengths are also summarized in Table 3. In parametric study, the initial beam length of 75 mm is chosen and it is reduced in steps of 5 mm until the criterion on the maximum strain is met. The beam length of 75 mm is chosen to show that the further increase in beam length beyond the original length of 70 mm will result in higher strain on the material. As the length of the beam increases, its stiffness decreases, resulting in higher deflection (strain) for the given vibration input. Hence, the parametric study is carried out by shortening the beam length to reduce the strain on material. An interesting finding from Figure 7(a) is that the peak power reduces with the shortening of beam, so is the strain on the beam. This behavior can be attributed to the diminishing influence of magnetic force on the increased stiffness of shorter beams. Another noticeable feature in Figure 7(a) is the increase in the average power near the resonant frequency of magnetic oscillator with the shortening of beam. In addition, longer beams have more significant shift in the natural frequencies of PEH and magnetic oscillator because of magnetic interaction, resulting in a dip of power in between the peaks. As the beam length reduces, the shift in resonant frequencies is not so significant. Moreover, the slightly higher damping of shorter beams helps in broadening of bandwidth and thus results in achieving better power output without having a dip in between the two peaks. The bandwidth given in Table 3 corresponds to the frequency range with more than 100μW power output (required by a wireless sensor) (Tang et al., 2010). With shortening of beams, the trade-off for reduction in the maximum power output is increase in the bandwidth. The improvement in bandwidth is minor for beam lengths less than 60mm. As shown in Figure 7(b), the maximum strain in the piezoelectric material increases with the beam length. For all the beams in the parametric with d=10 mm, the maximum strain is below the acceptable limit but they have lower bandwidth when compared to their counterparts with d=8 mm. For the beam lengths of 50mm and 55mm with d=8 mm, the maximum strain is within the acceptable limit. Out of these two alternatives, the beam length of 55mm with 8mm of spacing between magnets is taken as the optimal configuration as it has better combination of peak power and bandwidth. It is worth mentioning that the configuration L=75 mm, d=10 mm has higher power output than the optimal configuration (L=55 mm, d=8 mm) but has much lower bandwidth.

A constraint on the system mass affects the performance of the harvester and imposes a upper limit on the energy harvested (Kim et al., 2010; Shafer et al., 2012; Langley, 2014). The tip masses required for various lengths of the beams to keep natural frequencies of main beam and oscillator beam at 27.8 and 24.4 Hz, respectively, are also given in Table 3. It is quite evident from the table that the tip mass value increases with shortening of beam to keep same natural frequencies for the PEH and the oscillator. In this study, while choosing optimal configuration (L=55 mm, d=8 mm), only constraint on the material strength is considered. In case, the constraint on the system mass is also imposed and if the considered geometric parameters do not meet criteria of both system mass and material strength, a more comprehensive study is required. In such scenario, various thicknesses of beams along with various lengths should be considered in the parametric study to choose the optimal configuration. However, in the present work, only the constraint on the material strength of piezoelectric material is taken into consideration.

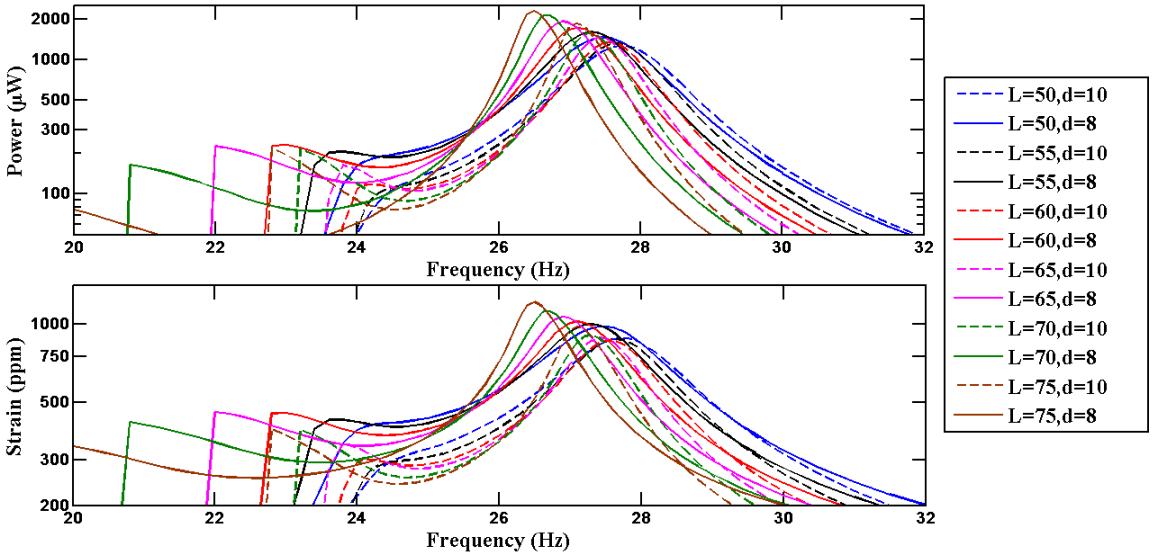

Figure 7. (a) Power and (b) strain curves for various configurations of nonlinear energy harvesters excited at a_{rms}=2m/s^2 and with d=8 and 10mm.

Table 3. Summary of results of parametric study.

	Linear harvester			Nonlinear harvester, d=10 mm			Nonlinear harvester, d=8 mm			Tip mass (g)	
L (mm)	Max power (μW)	Band width (Hz)	Strain (ppm)	Max power (μW)	Band width (Hz)	Strain (ppm)	Max power (μW)	Band width (Hz)	Strain (ppm)	Main beam	Oscillator beam
75	1153.6	2.7	748.3	1868.6	3.5	975.9	2315.7	3.6	1214.8	3.63	4.79
70	1079.9	3	737.0	1579.2	3.9	906.3	2137.5	4.3	1119.0	4.61	6.06
65	1085.3	3.5	753.8	1465.2	5.8	884.8	1926.0	7.1	1065.6	5.93	7.70
60	1076.7	3.9	768.4	1349.2	5.8	862.8	1725.9	6.7	1019.5	7.74	10.1
55	1108.4	4.7	801.5	1313.4	5.9	872.4	1600.0	6.7	997.4	10.3	13.4
50	1119.7	5.5	832.5	1261.8	6.3	880.6	1462.1	6.8	977.1	14.1	18.2

Experimental results

A nonlinear PEH is fabricated with the optimal configuration determined from the parametric study, i.e., L=55mm and d=8mm. For comparison purpose, experiment is also carried out on d=10mm and linear PEH. The overview of the experimental setup is shown in Figure 8(a). The base excitation to the nonlinear harvester is provided by the combination of a vibration exciter (APS 113), a function generator (RIGOL DG1011) and a power amplifier (APS model 116). The nonlinear PEH with magnetic oscillator is shown in Figure 8(b). The magnets are embedded in the tip masses attached to the end of the beams. Figure 8(b) shows the strain gauge (FLA 5-23-5L) used for measuring the strain on MFC patch. The strain data is acquired by dynamic strain meter (DRA 101C) using a resolution of 0.2ms. Experiments are conducted at a harmonic base acceleration of 2 m/s^2 (RMS). The RMS voltage is measured across the resistor while sweeping the frequency and power delivered to the resistor is calculated using the formula V^2_{rms}/R_L.

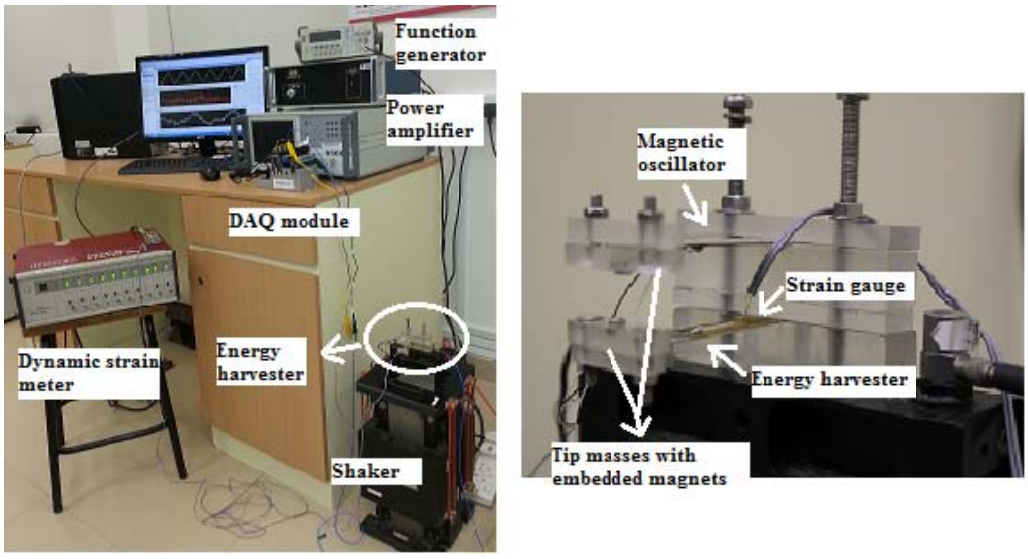

(a) (b)

Figure 8. (a) Entire experimental setup (b) Prototype of nonlinear energy harvester with magnetic oscillator

In Figure 9, power output of linear and nonlinear harvesters is plotted. Results of optimal configuration (L=55mm) are compared with the results of the previous study where beam length of 70mm was used (Tang and Yang, 2012). The power output from the linear configurations is shown in Figure 9(a). The optimal configuration has 21% higher power output in linear case. The power output from the linear harvester at resonance is proportional to mass, coupling coefficient and inversely proportional to damping (Erturk and Inman, 2008). It is obvious that the beam with L=55mm has higher tip mass than the beam with L=70mm to match natural frequency (27.8Hz). Additionally, coupling coefficient increases as the length of the beam decreases because of the increased slope of the mode shape in composite section. Though the optimal beam has higher damping (Figure 6), the combination of higher tip mass, coupling coefficient and damping results in the increased power output. It is obvious from Figure 9(b) that the optimal configuration has higher peak power and wider bandwidth as compared to the beam length of 70mm. The optimal configuration with L=55mm and d=8mm produces a peak power of 1658μW with a useful bandwidth of 6Hz, and has higher power output than the configuration of L=70mm and d=10mm for the most of the bandwidth. For L=55 mm, the natural frequency of the linear harvester is achieved at 27.7 Hz compared to the simulated value of 27.8 Hz. The presence of magnetic nonlinearity shifted the natural frequency from 27.7 Hz to 27.3 Hz and 26.3 Hz for d=10 mm and 8 mm, respectively. The experimentally measured strain in the piezoelectric material for linear and nonlinear harvesters is shown in Figure 10. The maximum strain (1023ppm) for the optimal configuration is just above the allowable limit (1000ppm) which is acceptable.

Finally in Figure 11, the comparison between theoretical and experimental power output from the optimal configuration for both linear and nonlinear PEH is shown. The power outputs from theoretical modeling and experiment are in good agreement for the linear PEH with 10% error in prediction of maximum power output. For the nonlinear PEH, the overall trend and power output is captured quite well by theoretical modeling, but there is an error of 0.9Hz in predicting resonant frequency. The peak power (1658μW) and maximum strain (1023ppm) of optimal configuration from the experiment are slightly higher than the theoretical predictions which are 1600μW and 997ppm, respectively. This is because of the slightly higher tip mass used in the

experiment than in the theoretical modeling to compensate for the additional stiffness due to the epoxy layer in between the substrate and piezoelectric material. The thickness of epoxy layer increases the distance of extreme piezoelectric layer from neutral axis, which results in excess of strain. In theoretical modeling, the damping ratio measured for linear case has also been used for nonlinear case. That is not exactly true as the damping ratio value changes for nonlinear case because of higher amplitudes and changes in the stiffness of beam because of magnetic interaction. Though extreme caution has been taken in conducting the experiments, a slight error in the alignment of magnets or the gap between magnets could affect the results. Moreover, the assumption of axial alignment (magnetization axis) of magnets during vibration is not so accurate because of considerable rotations of tip masses at the free end of cantilever beams. Additionally, the tip mass is assumed to be point mass without rotational inertia which is not the case in experiment. Considering these sources of error, we can say experimental results are in very good agreement with theoretical prediction.

Su et al. (2014) designed and experimentally tested a bistable dual-cantilever piezoelectric energy harvester which consists of an inner and an outer beam with magnets attached to their tips. Under a base acceleration of 3 m/s^2, the inner beam has produced a useful power output of 100μW between 14 to 16 Hz, with a peak power output of approximately 0.8 mW. The outer beam has useful power output between 9 to 11 Hz and a peak power output of 1 mW. Another design by Zhu et al. (2013), a buckled-beam piezoelectric energy harvester with a midpoint magnetic force produced an open circuit voltage of 5V (0-peak) between 20 to 23 Hz at a base acceleration of 0.2g. When compared with the above designs, the proposed optimal nonlinear harvester with magnetic oscillator generates useful power output between 23 to 29Hz with a much higher peak power of 1.66 mW under a base excitation of 0.2g_{rms} (2.83 m/s^2).

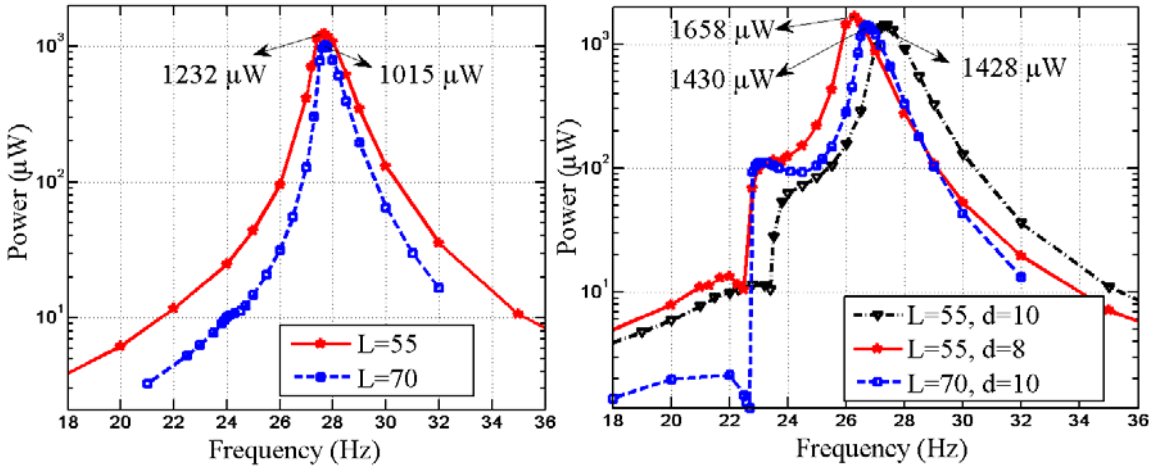

(a) (b)

Figure 9. Measured power output from (a) Linear and (b) Nonlinear energy harvesters excited at a_{rms}=2m/s^2.

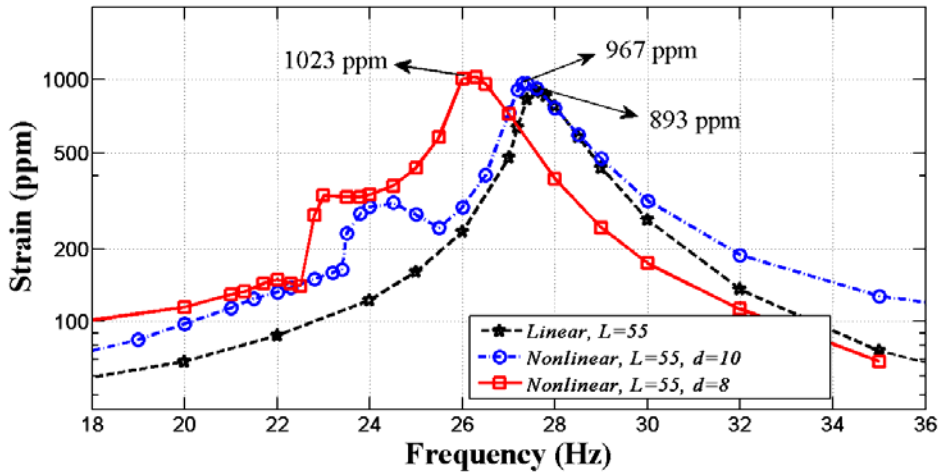

Figure 10. Measured strain on the piezoelectric material of linear and nonlinear energy harvesters excited at a_{rms}=2m/s^2.

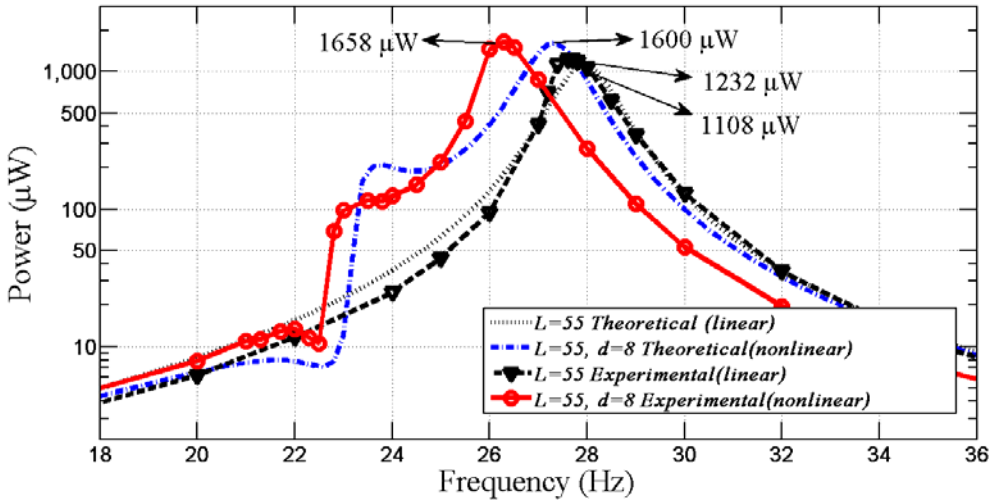

Figure 11. Experimental and theoretical power outputs of linear and nonlinear energy PEHs excited at a_{rms}=2m/s^2.

Conclusions

The authors believe that quest for enhancing the performance of nonlinear energy harvesters is not meaningful without taking material strength into consideration in the design process. In this paper, the performance of a nonlinear energy harvester with magnetic oscillator is optimized while imposing constraint on the material strength. The charge model is employed to calculate the force between permanent magnets and it is shown that the dipole model would give highly erroneous results when the distance between magnets is 7mm or less. The maximum strain on the cantilever beam is evaluated assuming small mechanical and electrical perturbations. Parametric study is carried out by varying the beam length and spacing between magnets of PEH and magnetic oscillator to seek the optimal configuration of nonlinear energy harvester. Experiments are carried out to validate the results of theoretical modeling. At a base acceleration of 2m/s^2 (RMS), the optimal energy harvester generates a peak power of 1658μW with a useful bandwidth of 6Hz and the maximum strain in piezoelectric material is 1023ppm.

Funding Acknowledgements

This research received no specific grant from any funding agency in the public, commercial, or not-for-profit sectors.

Notes

1. Morgan Advanced Materials. Properties of PZT bimorph available at : http://www.morganelectroceramics.com/products/piezoelectric/piezo-bimorphs/r6001_piezo_brochureweb.pdf (accessed on 22 October 2013)
2. Channel Industries, Inc. Properties of PZT patch available at : http://www.channelindustries.com/_includes/chan_cat.pdf (accessed on 22 October 2013)
3. MIDE Volture. Properties of PZT wafer available at : http://www.mide.com/pdfs/Volture_Datasheet_001.pdf (accessed on 22 October 2013)
4. Smart materials. Properties of MFC patch available at : http://www.smart-material.com/MFC-product-main.html (accessed on 22 October 2013)
5. TRS electrostrictors. Properties of PMN-PT patch available at : http://www.trstechnologies.com/pdf/Electrostrictors.pdf (accessed on 22 October 2013)
6. http://asm.matweb.com/search/SpecificMaterial.asp?bassnum=MA6061t6

References

Aboulfotoh NA, Arafa MH and Megahed SM (2013) A self-tuning resonator for vibration energy harvesting. *Sensors and Actuators A: Physical*

Agashe JS and Arnold DP (2008) A study of scaling and geometry effects on the forces between cuboidal and cylindrical magnets using analytical force solutions. *Journal of Physics D: Applied Physics*, 41(10), 105001.

Akoun G and Yonnet JP (1984) 3D analytical calculation of the forces exerted between two cuboidal magnets. *Magnetics, IEEE Transactions on*, 20(5), 1962-1964.

Al-Ashtari W, Hunstig M, Hemsel T and Sextro W (2012) Frequency tuning of piezoelectric energy harvesters by magnetic force. *Smart Materials and Structures*, 21(3), 035019.

Anton SR, Erturk A and Inman DJ (2010) Strength analysis of piezoceramic materials for structural considerations in energy harvesting for UAVs. *In Proc. of SPIE Vol* (Vol. 7643, p. 76430E).

Challa VR, Prasad MG, Shi Y and Fisher FT (2008) A vibration energy harvesting device with bidirectional resonance frequency tunability. *Smart Materials and Structures*, 17(1), 015035.

Elvin NG and Elvin AA (2009) A general equivalent circuit model for piezoelectric generators. *Journal of Intelligent Material Systems and Structures*, 20(1), 3-9.

Erturk A, Hoffmann J and Inman DJ (2009) A piezomagnetoelastic structure for broadband vibration energy harvesting. *Applied Physics Letters*, 94(25), 254102-254102.

Erturk A and Inman DJ (2008) On mechanical modeling of cantilevered piezoelectric vibration energy harvesters. Journal of Intelligent Material Systems and Structures, 19(11), 1311-1325.

Erturk A and Inman DJ (2011) *Piezoelectric energy harvesting*. Wiley.

Fett T, Munz D and Thun G (1999) Tensile and bending strength of piezoelectric ceramics. *Journal of Materials Science Letters*, 18(23), 1899-1902.

Furlani EP (2001) *Permanent magnet and electromechanical devices: materials, analysis, and applications*. Elsevier.

Hagood NW, Chung WH and Von Flotow A (1990) Modelling of piezoelectric actuator dynamics for active structural control. *Journal of Intelligent Material Systems and Structures*, 1(3), 327-354.

Harne RL and Wang KW (2013) A review of the recent research on vibration energy harvesting via bistable systems. *Smart Materials and Structures*, 22(2), 023001.

Kim M, Hoegen M, Dugundji J and Wardle BL (2010) Modeling and experimental verification of proof mass effects on vibration energy harvester performance, *Smart Materials and Structures*, 19(4), 045023.

Langley RS (2014) A general mass law for broadband energy harvesting, *Journal of Sound and Vibration*, 333(3), 927-936.

Leonard M (2001), *Fundamentals of vibrations*. Prentice Hall.

Lin J, Lee B and Alphenaar B (2010) The Magnetic Coupling of a Piezoelectric Cantilever for Enhanced Energy Harvesting Efficiency. *Smart Materials and Structure*, 19:045012.

Mann BP and Sims ND (2009) Energy harvesting from the nonlinear oscillations of magnetic levitation. *Journal of Sound and Vibration*, 319(1), 515-530.

Narita F, Shindo Y and Saito F (2007) Cyclic Fatigue Crack Growth in Three-Point Bending PZT Ceramics under Electromechanical Loading. *Journal of the American Ceramic Society*, 90(8), 2517-2524.

Pellegrini SP, Tolou N, Schenk M and Herder JL (2012) Bistable vibration energy harvesters: A review. *Journal of Intelligent Material Systems and Structures.*

Ravaud R, Lemarquand G, Babic S, Lemarquand V and Akyel C (2010) Cylindrical magnets and coils: Fields, forces and inductances. *Magnetics, IEEE Transactions on*, 46(9), 3585-3590.

Robertson W, Cazzolato B and Zander A (2011) A simplified force equation for coaxial cylindrical magnets and thin coils. *Magnetics, IEEE Transactions on*, 47(8), 2045-2049.

Schäufele AB and Heinz Härdtl K (1996) Ferroelastic properties of lead zirconate titanate ceramics. *Journal of the American Ceramic Society*, 79(10), 2637-2640.

Shafer MW and Garcia E (2013) Fundamental power limits of piezoelectric energy harvesters based on material strength. *In SPIE Smart Structures and Materials+ Nondestructive Evaluation and Health Monitoring* (pp. 86880D-86880D). *International Society for Optics and Photonics*.

Shafer MW, Bryant M and Garcia E (2012) Designing maximum power output into piezoelectric energy harvesters, *Smart materials and structures*, 21(8), 085008.

Sodano HA, Park G and Inman DJ (2004) Estimation of electric charge output for piezoelectric energy harvesting. *Strain*, 40(2), 49-58.

Standards Committee of the IEEE Ultrasonics, Ferroelectrics and Frequency Control Society (1987) IEEE standard on piezoelectricity, IEEE, New York.

Stanton SC, McGehee CC and Mann BP (2010) Nonlinear Dynamics for Broadband Energy Harvesting: Investigation of a Bistable Piezoelectric Inertial Generator. *Physica D*, 239:640653.

Stanton SC, McGehee CC and Mann BP (2009) Reversible hysteresis for broadband magnetopiezoelastic energy harvesting. *Applied Physics Letters,* 95:174103.

Su WJ, Zu J and Zhu Y (2014) Design and development of a broadband magnet-induced dual-cantilever piezoelectric energy harvester. *Journal of Intelligent Material Systems and Structures*, 25(4), 430-442.

Tang L, Yang Y and Soh CK (2010) Toward broadband vibration-based energy harvesting. *Journal of Intelligent Material Systems and Structures*, 21:1867.

Tang L, Yang Y and Soh CK (2012) Improving functionality of vibration energy harvesters using magnets. *Journal of Intelligent Material Systems and Structures*, 23(13), 1433-1449.

Tang L and Yang Y (2012) A nonlinear piezoelectric energy harvester with magnetic oscillator. *Applied Physics Letters*, 101(9), 094102-094102.

Twiefel J and Westermann H (2013) Survey on broadband techniques for vibration energy harvesting. *Journal of Intelligent Material Systems and Structures.*

Wickenheiser AM (2011) Design optimization of linear and non-linear cantilevered energy harvesters for broadband vibrations. *Journal of Intelligent Material Systems and Structures*, 22(11), 1213-1225.

Wilkie WK, High J and Bockman J (2002) Reliability testing of NASA piezocomposite actuators. Proceedings of the 8th International Conference on New Actuators, Bremen, Germany.

Zhu D, Roberts S, Tudor J and Beeby S. (2008) Closed Loop Frequency Tuning of a Vibration-based Microgenerator, *Proceedings of Power MEMS*, *Sendai, Japan*, pp. 229232.

Zhu Y and Zu JW (2013) Enhanced buckled-beam piezoelectric energy harvesting using midpoint magnetic force, *Applied Physics Letters*, 103(4), 041905.

Zhou S, Cao J, Erturk A and Lin J (2013) Enhanced broadband piezoelectric energy harvesting using rotatable magnets. *Applied Physics Letters*, 102(17), 173901-173901.

Appendix

Assuming variable substitution as below:

$$q_1(t) = u_1(t),\ q_2(t) = \dot{u}_1(t),$$
$$q_3(t) = u_2(t),\ q_4(t) = \dot{u}_2(t), \tag{20}$$
$$q_5(t) = V(t)$$

Using above variable substitution, the governing equations (11) to (13) can be written in state space form as

$$\dot{q}_1(t) = q_2(t),$$
$$\dot{q}_2(t) = -\frac{C_1}{M_1}q_2(t) - \frac{K_1}{M_1}q_1(t) - \frac{\Theta}{M_1}q_5(t) + \frac{F_{mag}}{M_1} + \frac{F_1(t)}{M_1},$$
$$\dot{q}_3(t) = q_4 \tag{21}$$
$$\dot{q}_4(t) = -\frac{C_2}{M_2}q_4(t) - \frac{K_2}{M_2}q_3(t) - \frac{F_{mag}}{M_2} + \frac{F_2(t)}{M_2},$$
$$\dot{q}_5(t) = \frac{\Theta}{C^s}q_2(t) - \frac{1}{RC^s}q_5(t)$$